Phys. Lett. B 879 (2026) 140563

Contents lists available at ScienceDirect

Physics Letters B

journal homepage: www.elsevier.com/locate/physletb

Letter

Observation of tensor-driven high-momentum neutrons in ^{16}O via (p,d) reactions and zero-degree deuteron momentum spectroscopy

X. Wang [a,b], H.J. Ong [c,d,e,b,f,*], S. Terashima [c,a,*], I. Tanihata [b,a], Y.K. Tanaka [g], H. Geissel [h,i,1], N. Aoi [b,2], Y. Ayyad [j], J. Benlliure [j], F. Farinon [i], H. Fujioka [k], J. Gellanki [l,m], C.L. Guo [n], E. Haettner [i], W.L. Hai [a], M.N. Harakeh [i,o], C. Hornung [h], K. Itahashi [f], R. Janik [p,1], N. Kalantar-Nayestanaki [o], R. Knöbel [h,i], N. Kurz [i], K. Miki [q], I. Mukha [i], T. Myo [r,b], T. Nishi [f], D.Y. Pang [a], S. Pietri [i], A. Prochazka [i], C. Rappold [s,i], M.P. Reiter [h], J.L. Rodríguez-Sánchez [j,3], C. Scheidenberger [i,h,t], H. Simon [i], B. Sitar [p], P. Strmen [p,1], B.H. Sun [a], K. Suzuki [b,u], H. Toki [b], H. Weick [i], E. Widmann [u], J.S. Winfield [i,1], X.D. Xu [c,d,i], J.W. Zhao [a],
Tensor-Force Collaboration and Super-FRS Experiment Collaboration

[a] School of Physics, Beihang University, Beijing, 100191, China
[b] Research Center for Nuclear Physics, The University of Osaka, Ibaraki, Osaka, 567-0047, Japan
[c] State Key Laboratory of Heavy Ion Science and Technology, Institute of Modern Physics, Chinese Academy of Sciences, Lanzhou, 730000, China
[d] School of Nuclear Science and Technology, University of Chinese Academy of Sciences, Beijing, 100049, China
[e] Joint Department for Nuclear Physics, Lanzhou University and Institute of Modern Physics, Chinese Academy of Sciences, Lanzhou, 730000, China
[f] Nishina Center for Accelerator-Based Science, RIKEN, 2-1 Hirosawa, Wako, Saitama, 351-0198, Japan
[g] High Energy Nuclear Physics Laboratory, RIKEN, 2-1 Hirosawa, Wako, Saitama, 351–0198, Japan
[h] Universität Giessen, Heinrich-Buff-Ring 16, Giessen, 35392, Germany
[i] GSI Helmholtzzentrum für Schwerionenforschung GmbH, Planckstraße 1, Darmstadt, 64291, Germany
[j] IGFAE, Universidade de Santiago de Compostela, E-15782 Santiago de Compostela, Spain
[k] School of Science, Institute of Science Tokyo, 2-12-1 Ookayama, Meguro, Tokyo, 152-8551, Japan
[l] KVI-CART, University of Groningen, Zernikelaan 25, Groningen, 9747 AA, the Netherlands
[m] Hansraj College, University of Delhi, Delhi-110007, India
[n] Department of Radiation Oncology, National Cancer Center/National Clinical Research Center for Cancer/Cancer Hospital, Chinese Academy of Medical Sciences and Peking Union Medical College, Beijing, 100021, China
[o] ESRIG, University of Groningen, Zernikelaan 25, Groningen, 9747 AA, the Netherlands
[p] Comenius University Bratislava, Mlynská dolina, Bratislava, 842 48, Slovakia
[q] Tohoku University Department of Physics, Graduate School of Science and Faculty of Science, Aza-Aoba 6-3, Aramaki, Aoba-ku, Sendai, Sendai, 980-8578, Japan
[r] General Education, Faculty of Engineering, Osaka Institute of Technology, Osaka, 535-8585, Japan
[s] Instituto de Estructura de la Materia, CSIC, Madrid, Spain
[t] Helmholtz Forschungsakademie Hessen fuer FAIR (HFHF), GSI Helmholtzzentrum für Schwerionenforschung, Campus Giessen, Giessen, 35392, Germany
[u] Stefan-Meyer-Institut für Subatomare Physik, Boltzmangasse 3, Vienna, 1090, Austria

ARTICLE INFO

Editor: Silvia Monica Lenzi

Keywords:
Tensor interactions
High-momentum components
Transfer reaction

ABSTRACT

The ^{16}O$(p,d)^{15}$O reaction has been studied at 0° using 403-, 604-, 907- and 1209-MeV protons, comparing cross sections populating positive- and negative-parity states in ^{15}O. Transitions to positive-parity states exhibit strong enhancement due to high-momentum neutrons, while negative-parity transitions show much smaller effects. The cross-section ratio between positive- and negative-parity states rises sharply with momentum transfer, matching theoretical predictions that include tensor interactions, particularly the peak near 2 fm^{-1}. These results highlight 0° neutron-pickup reactions as a sensitive probe for tensor-driven high-momentum components, paving the way for studies in exotic nuclei via radioactive beams.

* Corresponding authors.
E-mail addresses: onghjin@impcas.ac.cn (H.J. Ong), tera@impcas.ac.cn (S. Terashima).
[1] Deceased.
[2] Present address: Center for Nuclear Study, University of Tokyo, Tokyo 113-0033, Japan
[3] Present address: CITENI, Campus Industrial de Ferrol, Universidade da Coruña, E-15403 Ferrol, Spain

https://doi.org/10.1016/j.physletb.2026.140563
Received 11 February 2026; Received in revised form 13 May 2026; Accepted 15 May 2026
Available online 22 May 2026

Tensor and short-range repulsive interactions are pivotal in nuclear physics and nuclear astrophysics, driving phenomena beyond mean-field descriptions [1]. In atomic nuclei, the tensor interactions – arising mainly from pion exchange – generate strongly correlated nucleon-nucleon pairs, modify spin-orbit splitting, and reshape magic numbers in exotic nuclei [2,3]. Together with the short-range correlations (SRCs) – induced by the strong repulsive interactions between nucleons – the tensor correlations generate configuration mixing via two-particle-two-hole (2p-2h) excitations, producing high-momentum nucleon pairs [4,5]. These correlations critically impact spectral functions, quench single-particle strengths [6], and underpin nuclear saturation and the equation of state (EoS) [7]. Their astrophysical implications are profound: affecting the stiffness of the EoS, determining stellar radii and tidal deformabilities in neutron stars, and impacting neutrino opacities in supernovae and the synthesis of heavy elements via the r-process nucleosynthesis [8–11].

The discovery of S-D wave mixing in the deuteron [12,13], which explained its quadrupole moment [14], provided clear evidence of mixing of high-momentum nucleons in nuclei. Since then, mixing of nucleons with high momentum or in high-excitation orbitals and its effect on nuclear structure and response have been studied. This includes quenching of Gamow-Teller transition strengths and isovector magnetic moments [15–17]. Although tensor interactions are expected to play a key role, substantial contributions from exchange currents and Δ-hole effects hinder isolating and extracting their distinct effect. The isoscalar magnetic moments exhibit distinctive behavior, and are well explained by incorporating 2p-2h excitations induced by tensor interactions extending to very high-energy orbitals [18–20]. A similar anomaly observed in the isoscalar $M1$ transition has also been attributed to tensor interactions [21]. However, because these studies do not explicitly link high-excitation orbitals to high-momentum components, the impact of high-momentum components on these observables is unclear. While *ab initio* calculations reveal high-momentum nucleons in nuclei [5] and the crucial role of tensor interactions in reproducing spectra of light nuclei with $A \leq 12$ [22], their effect on individual states remains unresolved. Models like the tensor-optimized shell model (TOSM) [23] and antisymmetrized molecular dynamics [24], which include full 2p-2h configurations show promise but face challenges when applied to p-shell nuclei.

Experimentally, quasi-free electron [1,4,25–27] and proton [28–30] scatterings have been extensively used to study high-momentum nucleons in nuclei, revealing short-range correlated nucleon pairs with momenta above the Fermi momentum. These reactions measure nucleon momentum distributions, showing that a significant fraction of nucleons form strongly correlated pairs. Both electron- and proton-induced knockout studies consistently highlight the importance of tensor correlations and SRCs in understanding nuclear structure and nucleon dynamics at short distances. While electron scattering experiments on exotic nuclei [31] remain extremely challenging, proton-induced knockout reactions are often limited by low statistics as they require the simultaneous detection of multiple particles, thus hindering the understanding of tensor and SRC effects on individual states.

A recent ^{16}O(p,pd) experiment employing neutron-pickup kinematics revealed strong cross-section enhancement for the lowest 1^+ (S =1, T =0) state in ^{14}N at large momentum transfers. This observation provides direct evidence for the presence of tensor-driven high-momentum neutron-proton pairs in ^{16}O [32]. To investigate high-momentum neutrons in ^{16}O, an experiment employing the (p,d) reaction was performed at proton energies of 198, 295, and 392 MeV, with the deuteron detected at a laboratory angle of 10° [33]. Instead of examining the absolute cross sections populating individual states, two cross section ratios were studied: R_+ for the positive-parity state ($1/2^+$ or $5/2^+$) and R_- for the negative-parity state ($3/2^-$), both relative to the ground state. Their dependence on momentum transfer was compared, together with previous data [34–38], to identify tensor-induced reaction channels. While R_- increases slowly and saturates above 1 fm^{-1}, R_+ rises rapidly, indicating possible role of nucleon-nucleon correlations, especially those from tensor interactions. However, since these measurements were conducted at finite deuteron angles, the results may be subject to distortion effects and complexities arising from the reaction mechanism [39,40].

Previous studies have shown that the elastic $p+d$ scattering cross section at high proton energies exhibits a prominent peak in the backward direction, corresponding to deuteron emission at forward angles (e.g. [41,42]). This backward peak arises from an exchange process in which the incident proton picks up the neutron from the deuteron [43]. Because this is a two-body reaction, the momentum of the picked-up neutron is uniquely determined, allowing the experiment to probe the momentum distribution of the neutron inside the deuteron. Measurements at 0° are particularly valuable, since distortion effects and reaction-mechanism complexities are minimal at this angle [39,40]. Earlier theoretical studies attempted to explain minor irregularities observed in the extracted momentum distribution [44,45]. Later theoretical analysis showed that neutron momentum distribution extracted from high-energy 0° deuteron fragmentation experiments closely matches that obtained from $p+d$ elastic scattering [43]. This agreement demonstrates that backward scattering in $p+d$ elastic reactions reliably reflects the intrinsic momentum distribution of the neutron in the deuteron.

The cross section of the (p,d) reaction in the exchange-reaction domain (i.e., for deuteron emission angles near 0°) was investigated by Chew and Goldberger [46] within the framework of the Born approximation. Although their formulation was originally developed for (n,d) reactions, it applies equivalently to the (p,d) case. Within this framework, the reaction cross section is directly related to the overlap between the deuteron wave function and the internal neutron wave function of the target nucleus. The internal momentum of the picked-up neutron is given by $\vec{p}_n = \vec{k}_d - \vec{k}_p$, where $\vec{k}_p$ and $\vec{k}_d$ are the momenta of the incident proton and the emitted deuteron, respectively. The probed $\vec{p}_n$ therefore depends on both the incident proton energy and the deuteron scattering angle θ_d. To access neutron momenta around 2 fm^{-1} – a region where tensor-interaction effect is expected to dominate – at 0° scattering angle, a proton beam energy of approximately 800 MeV is required.

Here, we present the first measurement of the ^{16}O(p,d) differential cross sections at 0° using four incident beam energies ranging from 400 to 1200 MeV. Transitions to the negative-parity states of ^{15}O (the $1/2^-$ ground state and the $3/2^-$ state at 6.18 MeV), as well as the positive-parity $5/2^+$ state at 5.24 MeV, are reported.

The experiment was performed at GSI Helmholtzzentrum für Schwerionenforschung in Darmstadt, alongside the experiment reported in Refs. [47,48]. Proton beams from the SIS-18 synchrotron with energies of 403, 604, 907, and 1209 MeV were used to cover momentum transfer around 2 fm^{-1}. The proton beam bombarded a strip polyoxymethylene (POM; $(CH_2O)_n$) target with 1-mm horizontal width placed at the target station (TA) of the Fragment Separator (FRS) [49]. We used 100(3)- and 308(6)-mg/cm^2 thick POM targets for the measurements with the two lower- and two higher-energy proton beams, respectively. Other targets included 107(4)- and 327(1)-mg/cm^2 carbon for ^{12}C background subtraction, and 1027(2)-mg/cm^2 deuterated polyethylene (CD_2) for transmission efficiency calibration. Deuterons were momentum analyzed by the FRS in four added dispersive stages mode [50], and detected at the final focal plane (S4). The momentum dispersion at S4 was about 19 cm/%. Distinct magnetic rigidity settings were applied for the C and POM targets to cover states of interest at 403 MeV; a single rigidity setting sufficed for both targets at other energies. Detailed descriptions of the experiment conditions and detector setup are provided in Refs. [47,48] and elsewhere [51].

The horizontal position (X) distribution of the observed deuterons for the C and POM target measurement are shown in Fig. 1 (a)–(d) and (e)–(h), respectively. To achieve the best resolution, we applied corrections accounting for optical system aberrations and the shift of beam energy correlated with extraction time. At 403 MeV, except for the 6.18-MeV state in ^{15}O, which fully overlaps with the 2.00-MeV ($1/2^-$) state in ^{11}C, other ^{15}O states of interest are well resolved. For the data between 604 and 1209 MeV, the C-position spectra were first fitted with

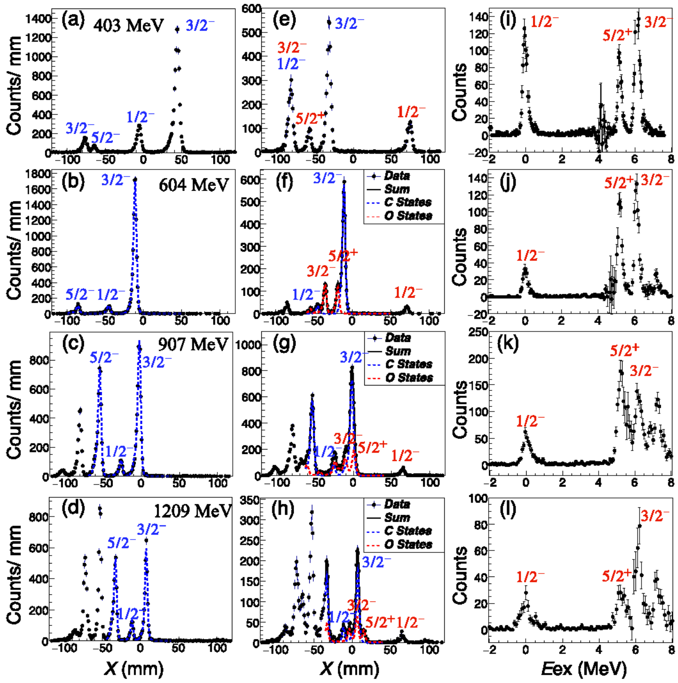

Fig. 1. Position spectra of carbon (a)–(d) and POM (e)–(h), and excitation-energy spectra of ^{15}O (i)–(l). Top panels show the data at 403 MeV (top), where discrete peaks are integrated individually without fitting. Lower panels show the data at higher incident energies: blue-dashed and red-dashed lines correspond to the ^{11}C- and ^{15}O-state fits, respectively; black-solid lines represent the overall fits.

double-Gaussian functions before being subtracted from the POM spectra. The relative height, peak-position difference and two widths defining the shape of the Gaussian functions were taken as free parameters but kept constant across all states. Focusing on the overlapping region, we fitted the ground state (g.s.; 3/2$^-$) and the 2.00(1/2$^-$)-, 4.32(5/2$^-$)-, and 4.80(3/2$^-$)-MeV excited states of ^{11}C, as shown by the blue-dashed lines in Fig. 1(b)–(d). Keeping the ^{11}C population ratios, the ^{15}O states were then fitted together with the ^{11}C states in the POM spectra, as shown by the red-dashed and blue-dashed lines, respectively, in Fig. 1(f)–(h). The black-solid lines represent the minimum-χ^2 fit to the POM spectra, determining the common shape parameters for both the ^{15}O and ^{11}C states, as well as the strength of the ^{11}C states. Several known low-lying excited states in ^{15}O: 5.24(5/2$^+$), 6.18(3/2$^-$), 6.79(3/2$^+$), 6.86(5/2$^+$), 7.28(7/2$^+$), 8.92(5/2$^+$), 9.66(3/2$^-$) and 10.30(5/2$^+$) MeV were included in the fitting, while the ground state was well separated and thus treated separately. We did not consider the 1/2$^+$ excited state at 5.18 MeV since the previous work [34] and conventional shell-model calculations indicate its contribution is negligible. Subtracting the fitted C spectra from the POM spectra, we obtained the ^{15}O position spectra. The deuteron momentum spectra were obtained from their linearly correlated X positions, allowing subsequent determination of ^{15}O excitation-energy spectra. The resultant ^{15}O excitation-energy spectra, with indicators for states of interest, are presented in Fig. 1(i)–(l), where corrections for the FRS transmission efficiency have been applied.

Due to the large momentum dispersion mode, the FRS momentum acceptance is non-uniform, requiring transmission efficiency corrections when subtracting ^{11}C components and determining (p,d) cross sections. We performed Monte Carlo simulations using MOCADI [52] with FRS optics from GICOSY [53] to model deuteron transport from TA to S4, incorporating beam profile, multiple scattering in the target, and beamline geometry. The simulations reproduced key optical properties – the phase space distributions, the dispersion and positions of the focal plane.

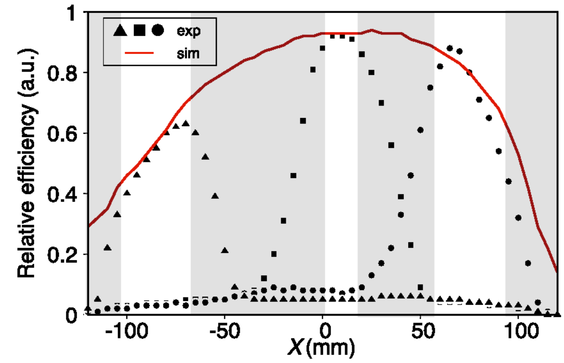

Fig. 2. Relative transmission efficiency of the FRS in the high-resolution mode from TA to S4. The black symbols and red line denote the experimental data and simulation results for CD$_2$-target, respectively. The data show the relative efficiency at the peak region, whereas the decline at the edges is attributed to the intrinsic width. Accordingly, the gray-shaded areas are excluded from the comparison.

A three-point magnetic rigidity scan was performed in CD$_2$-target measurements at 403 MeV to widen the momentum coverage of elastic pd scattering, as shown by the black symbols in Fig. 2. Since the amplitude near the peak center in each measurement reflects the relative efficiency, we normalized the simulated efficiency curve to the data. To better reproduce the experimental data, we multiplied the simulated data by a phenomenological quadratic distribution, and obtained the final distribution (red line). The difference between the corrected and original simulated data is taken as the systematic uncertainty. Similar simulations were performed at other energies.

To investigate possible tensor correlations in ^{16}O, we follow the previous work [33] and determine the ratios $R_- = \sigma(^{15}\mathrm{O}_{6.2})/\sigma(^{15}\mathrm{O}_{\mathrm{g.s.}})$ and $R_+ = \sigma(^{15}\mathrm{O}_{5.2})/\sigma(^{15}\mathrm{O}_{\mathrm{g.s.}})$, where $\sigma(^{15}\mathrm{O}_i)$ denotes the cross section of the transition to a certain final state i, as shown in Fig. 3. The horizontal axis shows the average momentum transfer, with the momentum transfer defined as $q \equiv |\vec{k_d} - \vec{k_p}|$, where $\vec{k_d}$ and $\vec{k_p}$ are momentum of deuteron and proton in laboratory system, respectively. Its uncertainty is defined as half the interval between the two corresponding momentum transfers. The filled symbols are the ratios from this work. The vertical error bars indicate the overall uncertainty, which includes the statistical and systematic uncertainties. The systematic uncertainty is attributed mainly to the uncertainty in the analysis procedures involving the spectral fitting and the C target spectrum subtraction (ranging from a few percent to about 20%), and the estimation of the transmission efficiency ($\leq$ 10%); the larger of these two contributions is adopted as the systematic uncertainty. The open symbols represent the experimental data from the literature, where the deuterons are measured at finite scattering angles. To avoid complication from reaction mechanism, we considered only data at deuteron-scattering angles $\leq$15° (in the center-of-mass system), obtained at various incident proton energies: 30 [54], 25–45 [34], 65 [35], 100 [36], 200 [37], 198, 295 and 392 [33], and 800 MeV [38]. Uncertainties are included where available.

The present data are in good agreement with the earlier results [33] at $q \simeq 1.5\,\mathrm{fm}^{-1}$. The discrepancy at $q \sim 2.2$ fm^{-1} between the present 0° data at 907 MeV (red-filled symbols) and the 10° data at 800 MeV (black-open symbols) from Ref. [38] suggests the possible influence of distortion effects. The ratio R_- changes gradually, varying by only a factor of 5 – less than an order of magnitude – across the range $0.3 \leq q \leq 2.7$ fm^{-1}. This behavior reflects population of both states through neutron pickup from the p-shell, whose wave functions are predominantly zero-particle-zero-hole (0p-0h) configurations and thus lack significant high-momentum components. In contrast, the ratio R_+ shows a dramatic increase by two orders of magnitude. Mean-field models cannot account for the population of sizable positive-parity states in direct transfer reactions, especially at high-momentum transfer. Tensor correlations,

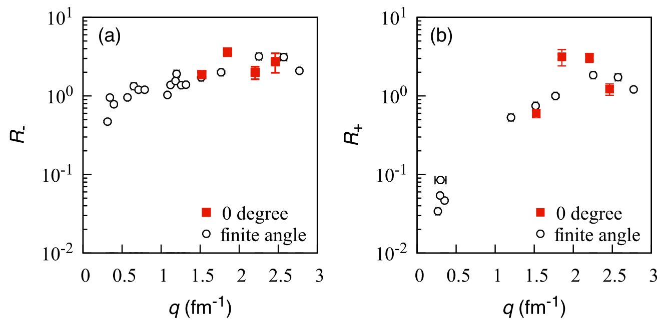

Fig. 3. Cross-section ratios R_- (a) and R_+ (b) versus momentum transfer q. Filled and open symbols indicate the results of present work at 0° and existing forward-angle data, respectively. See text for details.

obeying the selection rule $\Delta L = \Delta S = 2$, mix 2p-2h configurations with high-momentum components via promotion of a proton-neutron pair from the p- to the sd-shell, generating these states and explaining the observed rapid R_+ rise. A distinct peak at around $2\,\mathrm{fm}^{-1}$ in R_+ is observed exclusively in the 0° data, resembling the relative enhancement due to the tensor interactions predicted by various theoretical models [55–57].

In the earlier work by Ong et al. [33], a toy model using Gaussian basis wave functions for ^{4}He, constructed within TOSM as detailed in Ref. [58], was applied to calculate the momentum distribution ratio. This model describes the behavior of R_+ reasonably well, but fails to account for the peak at around $2\,\mathrm{fm}^{-1}$ revealed in the present work.

We compare R_+ with state-of-the-art theoretical calculations incorporating tensor interactions in ^{16}O [56,57,59,60]. While these models present the general features of nucleon momentum distributions in ^{16}O with and without tensor correlations, they currently lack orbital-by-orbital momentum distributions. This limitation prevents direct quantitative comparison with present data. We therefore assume that the momentum distribution is composed of two different components, namely central part ($n_\mathrm{C}(k)$) and tensor part ($n_\mathrm{T}(k)$). The full momentum distribution ($n_\mathrm{F}(k)$) is written as:

$$n_\mathrm{F}(k) = n_\mathrm{C}(k) + n_\mathrm{T}(k), \tag{1}$$

where k denotes the internal momentum of neutrons. Then, the momentum distributions of negative parity state ($n_-(k)$, the ground state in the present case) and positive parity state ($n_+(k)$, the $5/2^+$ excited state) can be written as:

$$n_-(k) = a_- n_\mathrm{C}(k) + b_- n_\mathrm{T}(k), \tag{2}$$

$$n_+(k) = a_+ n_\mathrm{C}(k) + b_+ n_\mathrm{T}(k). \tag{3}$$

where a_-, a_+, b_- and b_+ are unknown amplitudes associated with the observed states. The ratio R_+ is expressed as: $R_+(k) = n_+(k)/n_-(k)$. Since the negative parity states are mainly formed by 0p-0h configurations, where the contribution of the tensor interactions is considered negligible ($b_- \sim 0$), $R_+(k)$ can be reduced to:

$$R_+(k) \approx u + v\frac{n_\mathrm{T}(k)}{n_\mathrm{C}(k)}, \tag{4}$$

where $u = a_+/a_-$ and $v = b_+/a_-$.

To derive $n_\mathrm{T}(k)/n_\mathrm{C}(k)$, we use the MDs predicted by various models with distinct interactions. We adopt the MD without tensor interactions as $n_\mathrm{C}(k)$ and the one with tensor interactions as $n_\mathrm{F}(k)$. Taking the variational Monte Carlo (VMC) calculations with cluster expansion (Fig. 3, Ref. [59]) as an example, we extracted the MD from the dot-dashed line corresponding to the "Jastrow" wave function (with only central correlations) as $n_\mathrm{C}(k)$, and from the solid line representing the "Jastrow + two-body" as $n_\mathrm{F}(k)$, since the two-body cluster expansion primarily accounts for tensor correlations. The model ratio then becomes $n_\mathrm{T}/n_\mathrm{C} = n_\mathrm{F}/n_\mathrm{C} - 1$. We assume $n_\mathrm{T}/n_\mathrm{C} \approx 0$ at low momentum, where the tensor contributions are negligible compared with the central part. The renormalization of the central momentum distribution n_C is omitted in this analysis. The MDs calculated with and without tensor interactions are both normalized to the nucleon number ($A = 16$) in ^{16}O. While the central momentum distribution should ideally be renormalized to account for tensor-correlated nucleons, this effect is negligible compared to the observed orders-of-magnitude variation in R_+. Therefore, neglecting renormalization does not affect the physical interpretation of our results.

We assume that the ratio of cross sections for different final states reflects the ratio of the corresponding neutron momentum distributions. This assumption is supported by the Born approximation and our DWBA calculations. In the Born approximation, the (p,d) cross section is proportional to the probability of finding a neutron with momentum $\vec{q} = \vec{k}_d - \vec{k}_p$, where $\vec{k}_d$ and $\vec{k}_p$ are the momenta of the outgoing deuteron and the incident proton, respectively [46]. Thus, the cross section as a function of q directly represents the neutron momentum distribution in the target nucleus. In practice, however, the incoming and outgoing waves are distorted by nuclear potentials, which modifies this direct correspondence. To minimize such effects, we focus on small scattering angles at around 0°, where distortion is expected to be smallest, and analyze ratios of cross sections. DWBA calculations using global optical potentials indicate that the 0° cross section reproduces the momentum-distribution shape well, while deviations grow at larger angles. Detailed comparisons will be presented elsewhere [51]. Furthermore, distortion effects are nearly identical for different final states, since the incident energy is fixed and the outgoing deuteron energies differ only slightly between the ground and 5.2-MeV states, e.g. by about 1.3% and 0.4% at 403- and 1209-MeV incident energies, respectively. As a result, these effects are expected to largely cancel in the ratio R_+, suggesting that R_+ can be interpreted as a measure of the relative momentum components of the transferred neutrons. Hence, experimental $R_+(q)$ can be compared with $R_+(k)$, given u and v. Due to the absence of orbital-by-orbital calculations for ^{16}O including high-momentum components, we fix u and v using the experimental $R_+(q)$. At $q \sim 0\,\mathrm{fm}^{-1}$, $R_+ \approx u$, and thus $u = R_+^\mathrm{min} = 0.055$, considering the mean of the 22–45-MeV data [34]. The maximum value $R_+^\mathrm{max} \approx 3.1$ from the present work is used to determine $v = 0.29$ for VMC.

Fig. 4 shows the comparison of the experimental and theoretical R_+ ratios. The definition of symbols follows that of Fig. 3. Results of the VMC [59], the linked and number conserving cluster expansion (LNCCE) [57], and Fermi hypernetted chain (FHNC) [60] models are shown by the black-solid, red-dashed and magenta-dotted lines, respectively. For the LNCCE and FHNC models, we used the "Full" and "Central" lines (Fig. 2, Ref. [57]), and the "f_6" and "Jastrow" lines (Fig. 2, Ref. [60]) as $n_\mathrm{F}(k)$ and $n_\mathrm{C}(k)$, respectively. The blue lines show the ratios deduced using the distributions in Fig. 29 of Ref. [56] obtained with the unitary correlation operation method (UCOM); the line of "radial" is used as $n_\mathrm{C}(k)$ and the lines of three different range parameters for the tensor interactions – α, β and γ – are used as $n_\mathrm{F}(k)$, and the results are shown by the dash, dot-dashed, double-dot-dashed lines, respectively. The same u and v values obtained by VMC were adopted for all other models.

The experimental data and theoretical models exhibit good agreement, showing a peak in the ratio at momentum transfer near $2\,\mathrm{fm}^{-1}$, highlighting the dominant role of tensor contributions in the momentum-transfer dependence of the ratio. As momentum increases, the experimental ratio decreases, consistent with the findings from the recent electron-scattering study [27]. However, while theory predicts a sharp decline after the peak as momentum decreases, experimental ratios remain high down to lower momenta, dropping only a little. This unexpected behavior was also reported in Ref. [61], which studied ($S=1$, $T=0$) to ($S=0$, $T=1$) proton-neutron pairs in ^{4}He.

Deviation is also observed in the experimental data from Ref. [33], notably around $q \sim 1.2\ \mathrm{fm}^{-1}$. Since these experiments, including the data from Ref. [34], were performed near 10°, the discrepancy may

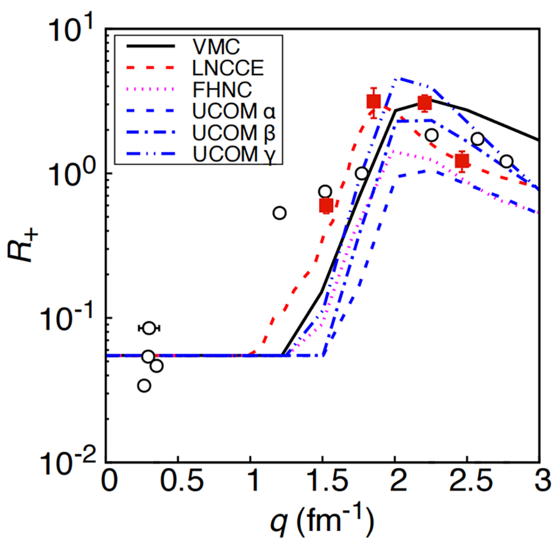

Fig. 4. Comparison of the cross-section ratios between experimental data and theoretical calculations. Filled symbols indicate the experimental data with the same definition as in Fig. 3. Lines represent the ratios deduced from theoretical calculations [56,57,59,60]. See text for further details.

stem from distortion effects, and therefore warrants further investigation. Indeed, DWBA calculations at 45 MeV [34,62] suggest the ratio rises sharply at small angles, indicating a much larger u. It is therefore desirable to obtain not only 0° experimental data at low energy, but also extend theoretical studies to include rigorous orbital-by-orbital calculations incorporating tensor interactions and high-momentum components to provide a more exclusive v value. It would be valuable to extend the renormalization-group method [63], which consistently treats both nuclear structure and reaction mechanisms, to the (p,d) reaction.

The ^{16}O$(p,d)^{15}$O reaction was studied at proton energies of 403, 604, 907, and 1209 MeV with deuterons detected at 0°. The cross-section ratios for populating ^{15}O excited states versus the ground state were systematically studied as a function of momentum transfer. A pronounced enhancement near $2\,\text{fm}^{-1}$ was observed for positive-parity state, attributed to tensor interactions that introduce high-momentum neutrons via two-particle-two-hole configuration mixing. Theoretical models incorporating tensor interactions show good agreement with experimental data, reproducing the peak structure at around $2\,\text{fm}^{-1}$ for the $5/2^+$-to-ground-state ratio. These results demonstrate that high-momentum neutron-pickup reactions at 0° are a sensitive probe for high-momentum components driven by the short-range nature of tensor interactions. The present findings open new avenues for investigating effects of tensor interactions in nuclei. Performing (p,d) reactions in inverse kinematics using intermediate- to high-energy radioactive beams at FAIR [64] and HIAF [65] to study exotic nuclei along isotopic and isotonic chains would be particularly valuable for elucidating the role of tensor interactions in shell evolution [2], intruder orbitals [66] and dense nuclear matter [7].

Data availability

Data will be made available on request.

Declaration of competing interest

The authors declare the following financial interests/personal relationships which may be considered as potential competing interests:

H.J. Ong, S. Terashima reports financial support was provided by National Natural Science Foundation of China. H.J.Ong reports financial support was provided by Chinese Academy of Sciences. H.J.Ong, S. Terashima reports financial support was provided by Gansu Provincial Science and Technology Department. I. Tanihata reports financial support was provided by Japan Society for the Promotion of Science. C.Scheidenberger reports financial support was provided by Hessian Ministry for Science and Art. C.Scheidenberger reports financial support was provided by Justus-Liebig-Universität Gießen and GSI. If there are other authors, they declare that they have no known competing financial interests or personal relationships that could have appeared to influence the work reported in this paper.

Acknowledgements

The authors acknowledge the support from various GSI departments, particularly the accelerator group and operators, the GSI target laboratory, and the engineers of the FRS group. X. W. acknowledges the support of scholarships from the Graduate School of Science, The University of Osaka and the Daiyukyo Foundation of International Exchange Assistance and Research. H. J. O. thanks M. Lyu, K. Ogata and T. Uesaka for inspiring discussion, and acknowledges the support of CAS President's International Fellowship Initiative. This work was supported by the Hessian Ministry for Science and Art (HMWK) through the LOEWE Center HICforFAIR, and by Justus-Liebig-Universität Gießen and GSI under the JLU-GSI strategic Helmholtz partnership agreement. Partial support was also provided by the JSPS Grant-in-Aid for Scientific Research No. 23224008, National Natural Science Foundation of China (12175009, 12175280), the International Partnership Program of the Chinese Academy of Sciences (016GJHZ2023063GC), and Major Science and Technology Projects in Gansu Province (24GD13GA005).

References

[1] O. Hen, et al., Nucleon-nucleon correlations, short-lived excitations, and the quarks within, Rev. Mod. Phys. 89 (4) (2017) 045002. https://doi.org/10.1103/RevModPhys.89.045002
[2] T. Otsuka, et al., Evolution of nuclear shells due to the tensor force, Phys. Rev. Lett. 95 (23) (2005) 232502. https://doi.org/10.1103/PhysRevLett.95.232502
[3] B.A. Brown, W.A. Richter, New "Magic numbers" for neutron-rich nuclei, Phys. Rev. C 74 (3) (2006) 034315. https://doi.org/10.1103/PhysRevC.74.034315
[4] R. Subedi, et al., Probing cold dense nuclear matter, Science 320 (2008) 1476. https://doi.org/10.1126/science.1156675
[5] R.B. Wiringa, et al., Nucleon and nucleon-pair momentum distributions in $A \le 12$ nuclei, Phys. Rev. C 89 (2) (2014) 024305. https://doi.org/10.1103/PhysRevC.89.024305
[6] L. Lapikas, Quasi-elastic electron scattering off nuclei, Nucl. Phys. A 553 (1993) 297c. https://doi.org/10.1016/0375-9474(93)90630-G
[7] W.H. Dickhoff, C. Barbieri, Self-consistent Green's function method for nuclei and nuclear matter, Prog. Part. Nucl. Phys. 52 (2) (2004) 377. https://doi.org/10.1016/j.ppnp.2004.02.038
[8] S. Gandolfi, et al., The maximum mass and radius of neutron stars and the nuclear symmetry energy, Phys. Rev. C 85 (3) (2015) 032801. https://doi.org/10.1103/PhysRevC.85.032801
[9] B.P. Abbott, et al., Measurements of neutron star radii and equation of state, Phys. Rev. Lett. 121 (16) (2018) 161101. https://doi.org/10.1103/PhysRevLett.121.161101
[10] L.F. Roberts, et al., Medium modification of the charged-current neutrino opacity and its implications, Phys. Rev. C 86 (6) (2012) 065803. https://doi.org/10.1103/PhysRevC.86.065803
[11] C.J. Horowitz, et al., R-process nucleosynthesis: connecting rare-isotope beam facilities with the cosmos, J. Phys. G 46 (8) (2019) 083001. https://doi.org/10.1088/1361-6471/ab0849
[12] J. Schwinger, On the neutron-proton interaction, Phys. Rev. 55 (1939) 235.
[13] W. Rarita, J. Schwinger, On the neutron-proton interaction, Phys. Rev. 59 (5) (1941) 436–452. https://doi.org/10.1103/PhysRev.59.436
[14] J.M.B. Kellogg, et al., The magnetic moments of the proton and the deuteron. the radiofrequency spectrum of H2 in various magnetic fields, Phys. Rev. 56 (1939) 728. https://doi.org/10.1103/PhysRev.56.728
[15] G.F. Bertsch, I. Hamamoto, Gamow-Teller strength at high excitations, Phys. Rev. C 26 (1982) 1323. https://doi.org/10.1103/PhysRevC.26.1323
[16] L.S. Towner, F.C. Khana, Quenching of allowed Gamow-Teller β transitions in mirror nuclei, Phys. Rev. Lett. 42 (1979) 51. https://doi.org/10.1103/PhysRevLett.42.51
[17] T. Wakasa, et al., Gamow-Teller strength of ^{90}Nb in the continuum studied via multipole decomposition analysis of the ^{90}Zr(p,n) reaction at 295 MeV, Phys. Rev. C 55 (6) (1997) 2909–2922. https://doi.org/10.1103/PhysRevC.55.2909
[18] K. Shimizu, et al., Magnetic moments and GT-type β-decay matrix elements in nuclei with a LS doubly closed shell plus or minus one nucleon, Nucl. Phys. A 226 (1974) 282. https://doi.org/10.1016/0375-9474(74)90407-2

[19] I.S. Towner, F.C. Khanna, Corrections to the single-particle M1 and Gamow-Teller matrix elements, Nucl. Phys. A 399 (1983) 334. https://doi.org/10.1016/0375-9474(83)90252-X
[20] A. Arima, et al., Isoscalar magnetic moments and the role of the δ-hole excitation, Hyperfine Interac. 21 (1985) 79. https://doi.org/10.1007/BF02061978
[21] H. Matsubara, et al., Nonquenched isoscalar spin-$M1$ excitations in sd-shell nuclei, Phys. Rev. Lett. 115 (10) (2015) 102501. https://doi.org/10.1103/PhysRevLett.115.102501
[22] S.C. Pieper, R.B. Wiringa, Quantum Monte Carlo calculations of light nuclei, Annu. Rev. Nucl. Part. Sci. 51 (2001) 53–90. https://doi.org/10.1146/annurev.nucl.51.101701.132506
[23] T. Myo, et al., Tensor-optimized shell model with bare nucleon-nucleon interaction for 4He, Prog. Theor. Phys. 121 (3) (2009) 511–531. https://doi.org/10.1143/PTP.121.511
[24] T. Myo, et al., New successive variational method of tensor-optimized antisymmetrized molecular dynamics for nuclear many-body systems, Prog. Theor. Exp. Phys. 2017 (2017) 073D01. https://doi.org/10.1093/ptep/ptx089
[25] O. Benhar, et al., Electron-scattering studies of correlations in nuclei, Rev. Mod. Phys. 65 (3) (1993) 817. https://doi.org/10.1103/RevModPhys.65.817
[26] K.I. Blomqvist, et al., Large recoil momenta in the D(e,e'p)n reaction, Phys. Lett. B 424 (1–2) (1998) 33–38. https://doi.org/10.1016/S0370-2693(98)00151-8
[27] A. Schmidt, et al., Probing the core of the strong nuclear interaction, Nature 578 (2020) 540. https://doi.org/10.1038/s41586-020-2021-6
[28] Y. Mardor, et al., Measurement of quasi-elastic 12C(p,2p) scattering at high momentum transfer, Phys. Lett. B 437 (3–4) (1998) 257–263. https://doi.org/10.1016/S0370-2693(98)01000-4
[29] A. Tang, et al., n-p short-range correlations from (p,2p + n) measurements, Phys. Rev. Lett. 90 (4) (2003) 042301. https://doi.org/10.1103/PhysRevLett.90.042301
[30] M. Patsyuk, et al., Unperturbed inverse kinematics nucleon knockout measurements with a carbon beam, Nat. Phys. 17 (2021) 693. https://doi.org/10.1038/s41567-021-01193-4
[31] T. Suda, H. Simon, Prospects for electron scattering on unstable, exotic nuclei, Prog. Part. Nucl. Phys. 96 (2017) 1. https://doi.org/10.1016/j.ppnp.2017.04.002
[32] S. Terashima, et al., Dominance of tensor correlations in high-momentum nucleon pairs studied by (p,pd) reaction, Phys. Rev. Lett. 121 (24) (2018) 242501. https://doi.org/10.1103/PhysRevLett.121.242501
[33] H.J. Ong, et al., Probing effect of tensor interactions in 16 O via (p,d) reaction, Phys. Lett. B 725 (4–5) (2013) 277–281. https://doi.org/10.1016/j.physletb.2013.07.038
[34] J.L. Snelgrove, E. Kashy, Energy dependence and spectroscopy of the ^{16}O(p,d)^{15}O reaction, Phys. Rev. 187 (4) (1969) 1246–1258. https://doi.org/10.1103/PhysRev.187.1246
[35] P.G. Roos, et al., The (p, d) reaction at 65 MeV, Nucl. Phys. A 255 (1) (1975) 187–203. https://doi.org/10.1016/0375-9474(75)90157-8
[36] J.K.P. Lee, et al., (p, d) reactions on light nuclei at 100 MeV, Nucl. Phys. A 106 (2) (1967) 357–368. https://doi.org/10.1016/0375-9474(67)90880-9
[37] R. Abegg, et al., Cross section and analyzing power measurements for the (p,d) reaction on ^{16}O and ^{40}Ca at 200 MeV, Phys. Rev. C 39 (1) (1989) 65–69. https://doi.org/10.1103/PhysRevC.39.65
[38] G.R. Smith, et al., (p,d) reaction at 800 MeV, Phys. Rev. C 30 (2) (1984) 593–615. https://doi.org/10.1103/PhysRevC.30.593
[39] J.V. Noble, H.J. Weber, On proton-deuteron backward elastic scattering at medium energies, Phys. Lett. 50B (2) (1974) 233–236. https://doi.org/10.1016/0370-2693(74)90546-2
[40] P. Berthet, et al., Elastic proton-deuteron backward scattering at energies from 0.6 to 2.7 GeV, J. Phys. G Nucl. Phys. 8 (8) (1982) L111. https://doi.org/10.1088/0305-4616/8/8/001
[41] G. Igo, J.C. Fong, S.L. Verbeck, M. Goitein, D.L. Hendrie, J.C. Carroll, B. McDonald, A. Stetz, M.C. Makino, Large-angle elastic scattering of deuterons from hydrogen: $Tk = 433$, 362 and 291 MeV, Nucl. Phys. A 195 (1) (1972) 33–56. https://doi.org/10.1016/0375-9474(72)90719-1
[42] J.C. Alder, W. Dollhoff, C. Lunke, C.F. Perdrisat, W.K. Roberts, P. Kitching, G. Moss, W.C. Olsen, J.R. Priest, Elastic pd scattering at 316, 364, 470, and 590 MeV in the backward hemisphere, Phys. Rev. C 6 (6) (1972) 2010–2019. https://doi.org/10.1103/PhysRevC.6.2010
[43] A.P. Kobushkin, Elastic proton-deuteron backward scattering in the one-nucleon-exchange approximation, J. Phys. G Nucl. Phys. 12 (6) (1986) 487–494. https://doi.org/10.1088/0305-4616/12/6/007
[44] J.C. Anjos, A. Santoro, F.R.A. Simão, D. Levy, Backward elastic pd scattering in the resonance energy region, Nucl. Phys. A 356 (2) (1981) 383–400. https://doi.org/10.1016/0375-9474(81)90196-2
[45] A.P. Kobushkin, M.V. Tokarev, Relativistic effects in the nucleon momentum distribution in the deuteron, J. Phys. G Nucl. Phys. 10 (1) (1984) L5. https://doi.org/10.1088/0305-4616/10/1/002
[46] G.F. Chew, M.L. Goldberger, The production of fast deuterons in high energy nuclear reactions, Phys. Rev. 77 (4) (1950) 470–475. https://doi.org/10.1103/PhysRev.77.470
[47] Y.K. Tanaka, et al., Measurement of excitation spectra in the ^{12}C(p,d) reaction near the η'-meson emission threshold, Phys. Rev. Lett. 117 (2016) 202501. https://doi.org/10.1103/PhysRevLett.117.202501
[48] Y.K. Tanaka, et al., Missing-mass spectroscopy of the ^{12}C(p,d) reaction near the η'-meson production threshold, Phys. Rev. C 97 (2018) 015202. https://doi.org/10.1103/PhysRevC.97.015202
[49] H. Geissel, et al., The GSI projectile fragment separator (FRS): a versatile magnetic system for relativistic heavy ions, Nucl. Instrum. Methods Phys. Res. Sect. B 70 (1–4) (1992) 286–297. https://doi.org/10.1016/0168-583X(92)95944-M
[50] E. Haettner, et al., New high-resolution and high-transmission modes of the FRS for FAIR phase-0 experiments, Nucl. Instrum. Methods Phys. Res. Sect. B 463 (2020) 455–459. https://doi.org/10.1016/j.nimb.2019.04.025
[51] X. Wang, et al. (in preparation).
[52] N. Iwasa, et al., MOCADI, a universal Monte Carlo code for the transport of heavy ions through matter within ion-optical systems, Nucl. Instrum. Methods Phys. Res., Sect. B 126 (1–4) (1997) 284–289. https://doi.org/10.1016/S0168-583X(97)01097-5
[53] H. Wollnik, B. Hartmann, M. Berz, Principles of GIOS and COSY, AIP Conf. Proc. 177 (1988) 74–85. https://doi.org/10.1063/1.37817
[54] N.S. Chant, et al., Asymmetries and differential cross sections for the 12C(p, d)11C and 16O(p, d)15O reactions induced by polarized protons, Nucl. Phys. A 99 (4) (1967) 669–685. https://doi.org/10.1016/0375-9474(67)90378-8
[55] R. Schiavilla, et al., Tensor forces and the ground-state structure of nuclei, Phys. Rev. Lett. 98 (13) (2007) 2–5. https://doi.org/10.1103/PhysRevLett.98.132501
[56] T. Neff, H. Feldmeier, Tensor correlations in the unitary correlation operator method, Nucl. Phys. A 713 (3–4) (2003) 311–371. https://doi.org/10.1016/S0375-9474(02)01307-6
[57] M. Alvioli, et al., Proton-neutron and proton-proton correlations in medium-weight nuclei and the role of the tensor force, Phys. Rev. Lett. 100 (16) (2008) 162503. https://doi.org/10.1103/PhysRevLett.100.162503
[58] T. Myo, et al., Tensor correlation in ^{4}He with the tensor-optimized shell model, Prog. Theor. Phys. 117 (2) (2007) 257. https://doi.org/10.1143/PTP.117.257
[59] S.C. Pieper, et al., Variational calculation of the ground state of ^{16}O, Phys. Rev. C 46 (5) (1992) 1741–1756. https://doi.org/10.1103/PhysRevC.46.1741
[60] A. Fabrocini, G. Co', One-body density matrix, natural orbits, and quasihole states in ^{16}O and ^{40}Ca, Phys. Rev. C 63 (4) (2001) 044319. https://doi.org/10.1103/PhysRevC.63.044319
[61] K. Miki, et al., Study of tensor correlations in 4He via the 4He(p, dp)d and 4He(p, dp)pn reactions, Few-Body Syst. 54 (7–10) (2013) 1353–1356. https://doi.org/10.1007/s00601-013-0611-7
[62] W.L. Hai, et al., (in preparation).
[63] A.J. Tropiano, S.K. Bogner, R.J. Furnstahl, Short-range correlation physics at low renormalization group resolution, Phys. Rev. C 104 (3) (2021) 034311. https://doi.org/10.1103/PhysRevC.104.034311
[64] FAIR–facility for antiproton and ion research, https://fair-center.eu/.
[65] X.H. Zhou, et al., Status of the high-intensity heavy-ion accelerator facility in China, AAPPS Bull. 32 (2022) 35. https://doi.org/10.1007/s43673-022-00064-1
[66] T. Myo, et al., Systematic study of 9,10,11Li with the tensor and pairing correlations, Prog. Theor. Phys. 119 (4) (2008) 561–581. https://doi.org/10.1143/PTP.119.561